ARTICLE

Triboelectric Nanogenerator as a Probe for Measuring the Charge Transfer between Liquid and Solid Surfaces

Jinyang Zhang,[§] Shiquan Lin,[§] Mingli Zheng, and Zhong Lin Wang*

Cite This: https://doi.org/10.1021/acsnano.1c04903

Read Online

ACCESS | Metrics & More | Article Recommendations | SI Supporting Information

ABSTRACT: The phenomenon of triboelectricity involves the flow of charged species across an interface, but conclusively establishing the nature of the charge transfer has proven extremely difficult, especially for the liquid−solid cases. Herein, we developed a self-powered droplet triboelectric nano-generator (droplet-TENG) with spatially arranged electrodes as a probe for measuring the charge transfer process between liquid and solid interfaces. The information on the electric signal on spatially arranged electrodes shows that the charge transfer between droplets and the solid is an accumulation process during the dropping and that the electron is the dominant charge-transfer species. Such a droplet-TENG showed a high sensitivity to the ratio of solvents in the mixed organic solution, and we postulated this is due to the possibility of generation of a hydrogen bond, affecting the electric signal on the spatially arranged electrodes. This work demonstrated a chemical sensing application based on the self-powered droplet triboelectric nanogenerator.

KEYWORDS: contact electrification, liquid−solid, probe, electron transfer, triboelectric nanogenerator
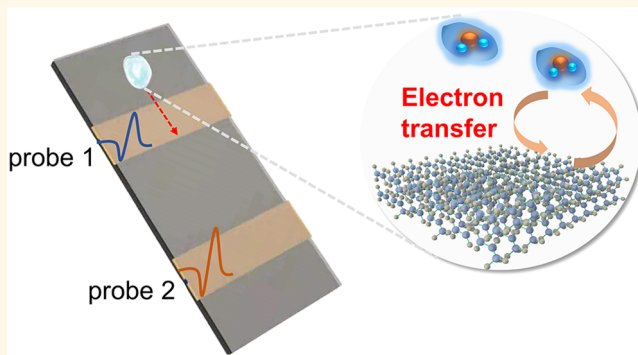
INTRODUCTION

When two materials are brought into contact and then separated, both of them become statically charged.[1,2] One surface develops a net positive charge, while the other acquires a net negative charge. This phenomenon, termed contact- or tribo-electrification,[3−6] is an old subject[7] and has widespread practical applications, such as a car static zip and the transfer of inks in xerography;[8] it occurs not only between solid−solid interfaces but also between liquid−solid interfaces.[9−12] Despite our familiarity with the phenomenon, we are still without a complete picture of its origin,[13,14] especially for liquid−solid interfaces.[15,16] Controversy remains over the charge transfer species (ion[17] or/and electron[18−20] transfer) and how charge transfers between liquids and solid surfaces.

In recent years, several studies have probed charge densities and species at the liquid−solid interface with the droplet triboelectric nanogenerator (droplet-TENG),[21−23] which harvest energy from the motion of dropping water. Such water-driven droplet-TENGs have obvious advantages over the traditional solid TENG, such as abundant resources, from rivers to vast ocean waves.[24] Moreover, it provides the great opportunity to better study the origin of charge transfer between solid and liquid interfaces. Most research focuses on the one-electrode droplet-TENG,[25,26] which can be used to probe the dynamic process of charge accumulation for liquid−solid contact electrification in which multiple droplets contact with, slide down, and then separate from a hydrophobic polymer surface,[27] for example, polytetrafluoroethylene (PTFE). However, the use of only one metallic electrode beneath the hydrophobic polymer surface would provide limited information regarding the process of liquid−solid contact electrification.[27] For instance, failing to continuing monitoring the charge-transfer rate across the entire footprint of the water-dropping process. Some research works are devoted to developing a droplet-TENG with more than one metallic electrode; for example, the water droplet-TENG with a hybrid of a grating electrode and a single-electrode[28] can identify the time interval for the liquid flow and the number of
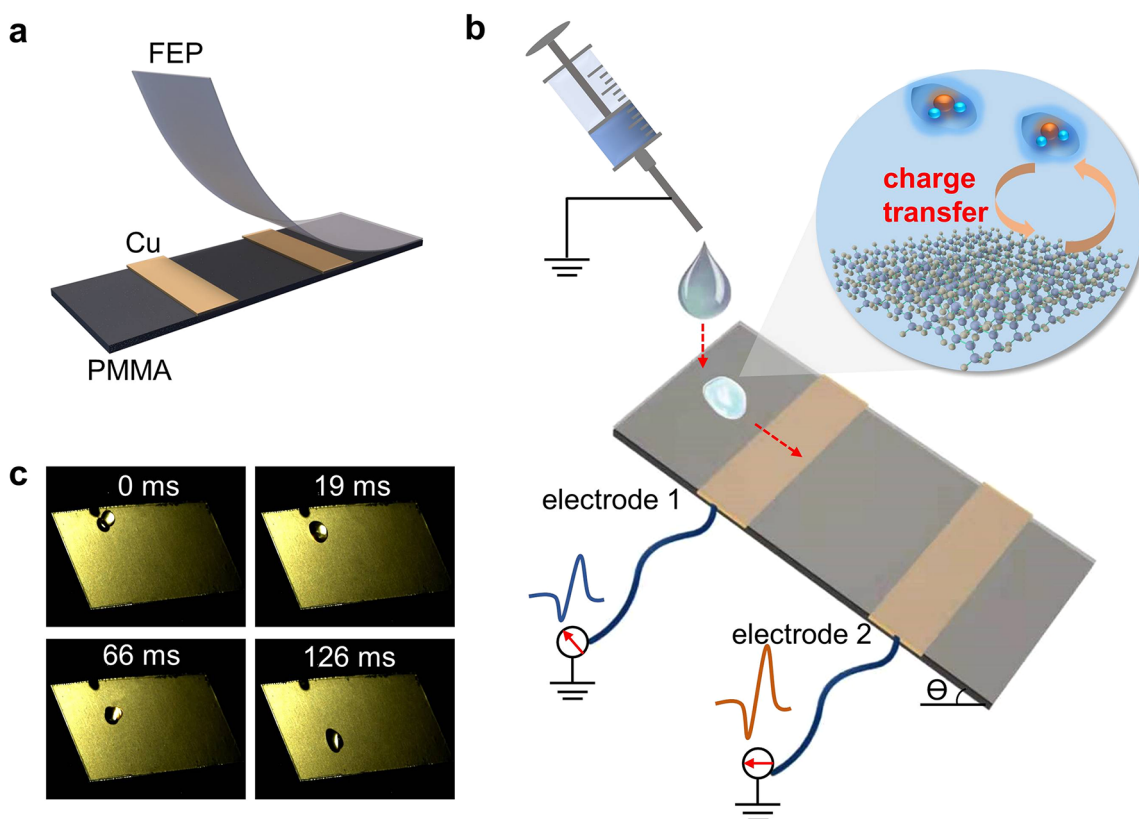
Figure 1. Experimental setup of droplet-TENG with spatially arranged electrodes. (a) Structure of the droplet-TENG: the bottom layer is a PMMA plate (backboards), and the top layer is dielectric polymer film for contact electrification with liquid droplets; Cu electrodes are located between PMMA and polymer film. (b) Working mechanism of the droplet-TENG. When a drop of liquid flows through the polymer surface, the charge transfer between liquid and solid occurred, and the current signals were measured by the two Cu electrodes separately. (c) Snapshots showing the motion of a water droplet sliding over the FEP film.

droplets. It is certain that such types of hybrid water droplet-TENG with multiple parallel electrodes can greatly improve the performance of TENG,[29−32] but it cannot analyze the signal on each separate single electrode. Information on the charge-transfer rate at different dropping times and on electric signal difference between separated electrodes is at present not accessible.

In this work, we have developed a simple self-powered droplet-TENG with spatially arranged metallic electrodes. The information on electric signal on spatially arranged electrodes provides the chance to probe the charge transfer between liquid and solid surfaces. This work provides evidence indicating that the dominant charge-carrying species, accounting for statics between liquid and polymers, are electrons. Further, such a droplet-TENG showed a high sensitivity to chemical sensing, such as the different concentrations of electrolytes in organic solution and the ratio of various substances in a mixed organic solution. We postulated the possibility of generation of hydrogen bonds affects the electric signal on spatially arranged electrodes and thus affects charge transfer. This study successfully validated the hypothesis that the liquid droplet-TENG may present a liquid sensing strategy for chemical sensor development.

RESULTS AND DISCUSSION

Figure 1a shows the fabrication of droplet-TENG, which consists of three layers: the bottom layer is a poly(methyl methacrylate) (PMMA) plate as the backboards, while the top layer is dielectric polymer film for contact electrification with

liquid droplet, such as fluorinated ethylene propylene (FEP), polytetrafluoroethylene (PTFE), kapton, and polyethylene (PE). The spatially arranged copper electrodes are attached between the polymer film and PMMA plate for electrostatic induction. The water contact angles for these polymers are shown in Figure S1, and all of them show a certain degree of hydrophobicity. Thus, water droplets easily slip off the surface of these inclined materials. Figure 1b shows the experimental design, where a liquid droplet (30 μL per drop) was released from a grounded stainless-steel needle (3 mm diameter) by a syringe pump at a fixed height (0.8 cm) above the polymer surface with a tilted angle. The two electrodes are probes for charge transfer and thus chemical sensing, for example, the ratio of solvents in a mixed organic. The movement of a water droplet was recorded by a fast camera at the rate of 1000 frames per second in Figure 1c. It shows the selected snapshots of a water droplet sliding across the FEP surface at the tilted angle θ of 60°. After the water droplet detaches from the needle, it immediately contacts with the polymer surface. As shown in Figure 1c, during the process of dropping, the water droplet has been kept in contact with the polymer surface. The water droplets drop in alternate shapes of stretching ($t = 19$ ms), contraction ($t = 66$ ms), and stretching ($t = 126$ ms).

Two spatially arranged copper electrodes connected to a grounded electrometer measure the induced current obtained from the interaction between the liquid droplet and the fresh polymer surface (Figure 1b). The values of the current peak and the induced charges for one liquid droplet upon contacting and separating with the copper electrode position are denoted
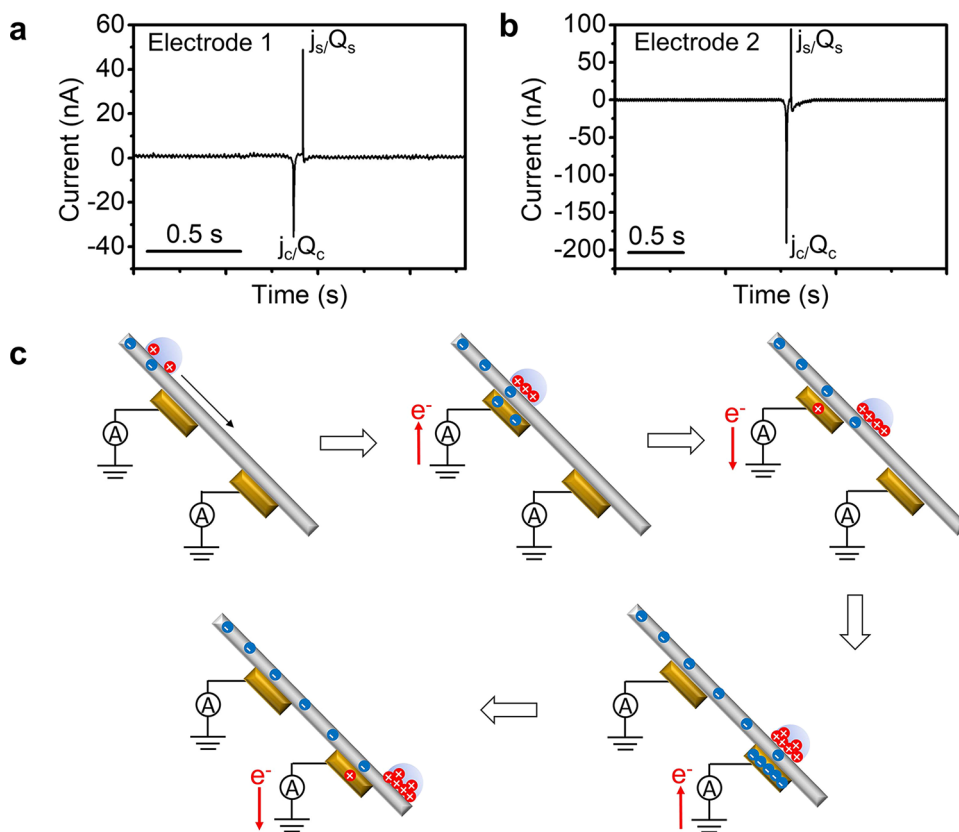
Figure 2. Working mechanism of the droplet-TENG with spatially arranged electrodes, electrode 1 and electrode 2. (a and b) A typical current output profile of the droplet-TENG on electrode 1 and electrode 2 when a water droplet contacted and separated with FEP film with Cu electrodes under it. j_c and j_s refer to the induced current, while Q_c and Q_s refer to the induced charge at the contacting or separating process of one droplet, respectively. (c) Schematic illustration of the working principle of the droplet-TENG for sensing a droplet at two electrodes.

as j_c, Q_c, j_s, Q_s, respectively. When the first droplet of water starts to touch the FEP film with the copper electrode beneath it, an induced current j_c (-37 nA for electrode 1 and -192 nA for electrode 2) was measured (Figure 2a,b); after the current peak is integrated, the corresponding transferred charge Q_c (-0.1 nC for electrode 1 and -1.8 nc for electrode 2) was calculated. Similarly, we can get the corresponding transferred charge Q_s (0.3 nC for electrode 1 and 0.5 nc for electrode 2) when the droplet separated from the polymer surface with the copper electrode beneath it. The difference between Q_c and Q_s ($\|\mid Q_s\mid - \mid Q_c\mid\|$), here denoted as q_1 (0.2 nC) for electrode 1 and q_2 (1.3 nC) for electrode 2, indicate the transferred charges on electrode 1 and electrode 2, respectively. Therefore, the transferred charge (Δq) between electrode 1 and electrode 2 was obtained, which can be calculated from $q_2 - q_1$ (1.1 nC). The physical meaning of Δq is the difference of the amount of charge transfer between two different points in the process of the water droplet falling from the FEP slope. Then the values of the average charge density for the first water droplet on electrode 1 ($\Delta\sigma_1$, nC cm^{-2}) and electrode 2 ($\Delta\sigma_2$, nC cm^{-2}) were calculated from the droplet sliding track ($A = 2 \times 0.5$ cm^{-2}), that is, $\Delta\sigma = q/A$. Here, $\Delta\sigma_1$ is 2 μC m^{-2}, while $\Delta\sigma_2$ is 13 μC m^{-2}.

The working mechanism of the droplet-TENG with two electrodes is proposed in Figure 2c. When the water droplet is sliding on the FEP film, the electrons will flow from water droplet to FEP film (because FEP has a strong affinity to electrons[33]), with the result being a positively charged water

droplet and a negatively charged FEP film (Figure 2c), while the positively charged water was started from losing an electron and becomes a cationic hole (H_2O^+) in a quite short lifetime (Figure S2).[34] Then the H_2O^+ cation joins with a neighboring water molecule to yield an OH radical and H_3O^+, according to the chemical reaction of the ionization of liquid water: $H_2O^+ + H_2O \rightarrow OH + H_3O^+$.[35] The charges on the water droplet continues to accumulate during the sliding on the FEP surface. When the water droplet slides over the position of electrode 1, the excess charge on the water droplet leads to the induced charge on the copper electrode 1, while after the water droplet separates from the position of electrode 1, the excess charge on the FEP surface leads to another induced charge. This is similar when the water droplet slides over the position of electrode 2, but as the water droplets fall, charge on the water droplet continues to accumulate, probably resulting in charge saturation on the water droplet when it slides over electrode 2; the electrons would then transfer from FEP to the water droplet, leading some induced negative charges to stay on electrode 2.[27] This is probably the reason for a smaller current peak j_s for electrode 2.

However, as the droplet number increase, the transferred charges between the FEP surface and water droplet decrease on both electrode 1 and electrode 2 (Figures 3a,b and S3). This is because the charge saturation prevents the further transfer of electrons between the FEP film and the water droplet.[27] Therefore, in our experiments, the first droplet of liquid was used to avoid the charge saturation effect.
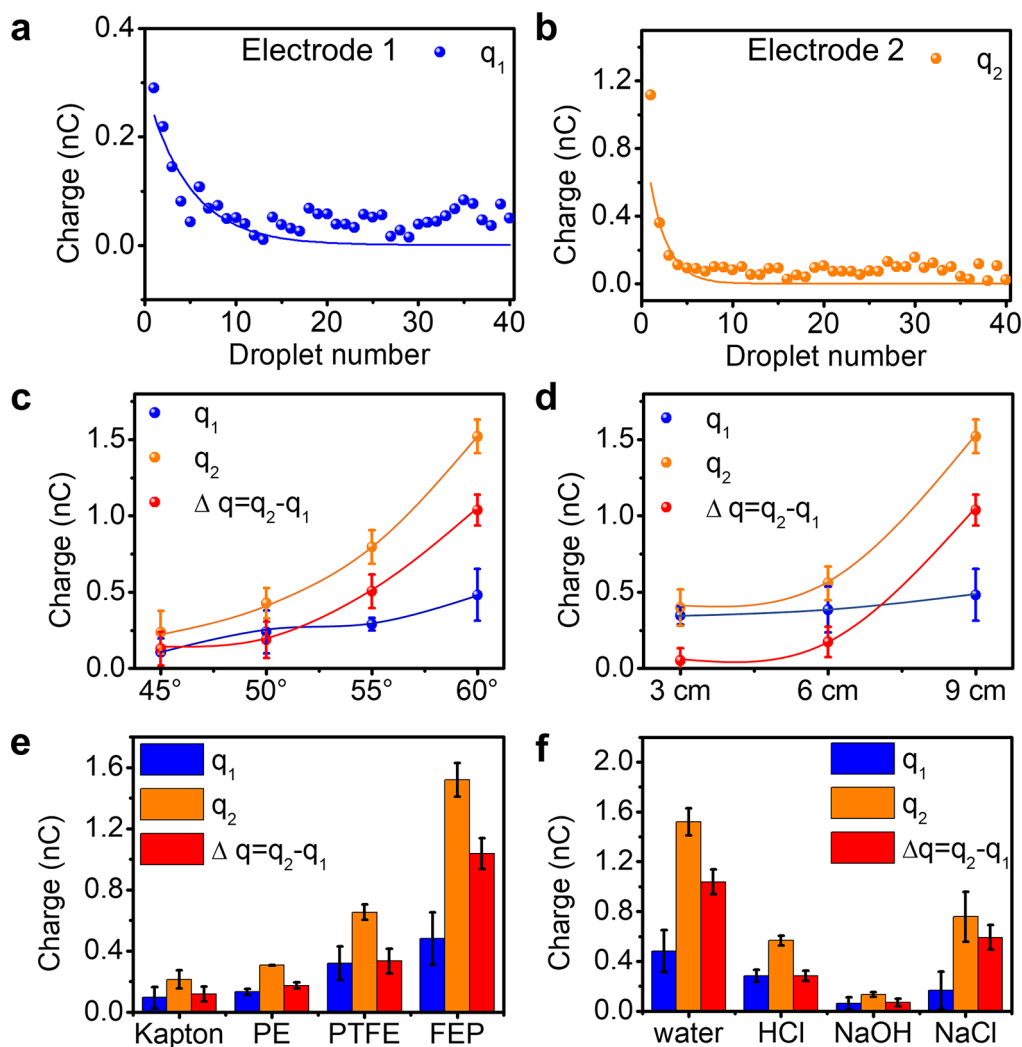
Figure 3. Electricity generation performance of liquid droplets sliding over the dielectric polymer films. (a and b) Electricity generation performance for electrode 1 and electrode 2 of FEP film contacted with hundreds of sequential water droplets. Transferred charge q recorded by an electrometer. $q = ||Q_s| - |Q_c||$. (c and d) The transferred charges on electrode 1 (q_1) and 2 (q_2) for water droplet sliding over the FEP surface, as well as the transferred charge between two electrodes (Δq), at different dropping angle and different distance between two electrodes. (e) The transferred charges of water droplet sliding over Kapton, PE, PTFE, and FEP. (f) The transferred charges of the original FEP with different droplets: water, HCl (pH 3), NaOH (pH 13), and NaCl (0.5 M).

The relationship between the tilted angle θ and the amount of transferred charge has been studied. For water droplets sliding on the hydrophobic materials, the dropping speed generally increases with surface tilted angle θ as the increasing of accelerated speed. Our data in Figure 3c quantify the transferred charge by tribocharging between the FEP film and the water droplet when the water droplet slides from electrode 1 to electrode 2 at different tilted angle (θ) of 45°, 50°, 55°, and 60°. The transferred charges on both electrode 1 and electrode 2 scale in proportion to the tilted angle θ (Figure 3c, blue and orange dots). Further, the transferred charge from electrode 1 to electrode 2 (Figure 3c, red dots), Δq, obviously increases from 45° to 60°. We note that the contact area between the water droplet and the FEP film has an impact on the accumulation of transferred charges. From the selected snapshots of a water droplet sliding across the FEP surface at different tilted angles (Figure S4), the water droplets of relatively smaller tilted angles (θ is 45°, 50°, or 55°) show only a hemispherical stretched morphology when sliding across the FEP surface with the slow sliding rate (Figure S4). However,

when the tilted angle θ is 60°, the sliding rate is faster compared with that of smaller tilted angles, and the water droplet drops in alternate shapes of stretching (t = 19 ms), contraction (t = 66 ms), and stretching (t = 126 ms). We propose these alternate shapes of the water droplet at θ = 60° increase the fresh contact area between the FEP film and the water droplet, thus enhancing the electron transfer. The distance between electrode 1 and electrode 2 was also considered. When the distance between electrodes 1 and 2 is relatively smaller, such as 3 or 6 cm, the transferred charges, q_1 and q_2, on both electrodes are smaller (less than 0.7 nC) compared with that when the length is 9 cm (approximately 1.5 nC) (Figure 3d). When the transferred charges, $\Delta q = q_2 - q_1$, between electrodes 1 and 2 of different sliding distances are compared, what becomes apparent is that the transferred charge scales with the sliding distance and accumulates as the water droplet slides off the FEP surface. This phenomenon was observed not only for the FEP film but also for many dielectric polymers, such as polytetrafluoroethylene (PTFE), kapton, and polyethylene (PE) (Figure 3e). FEP and PTFE have a stronger
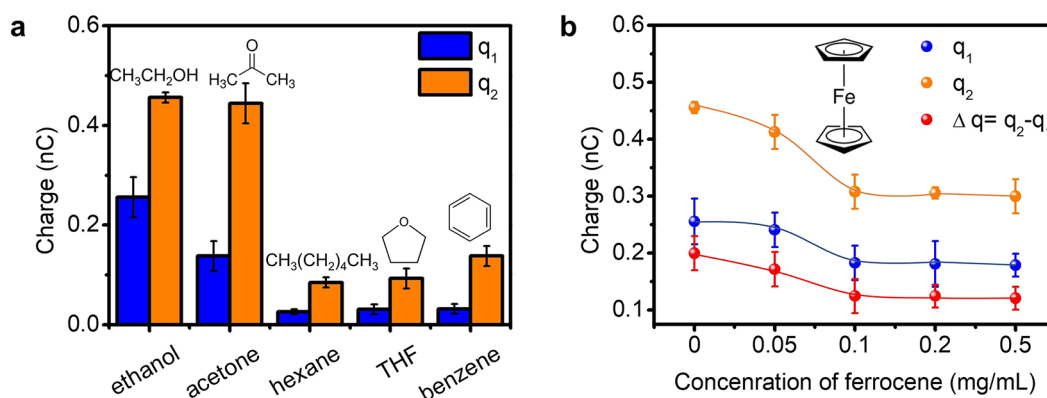
Figure 4. Sensing sensitivity of droplet-TENG to different organic solvents and concentration of ferrocene. (a) The transferred charges on electrode 1 (q_1) and 2 (q_2) for different organic droplets sliding over the FEP surface, including ethanol, acetone, hexane, THF, and benzene. (b) The transferred charges on electrodes 1 (q_1) and 2 (q_2) of ethanol/ferrocene droplet sliding over the FEP surface, as well as the transferred charge between two electrodes (Δq) as a function of the concentration of ferrocene.
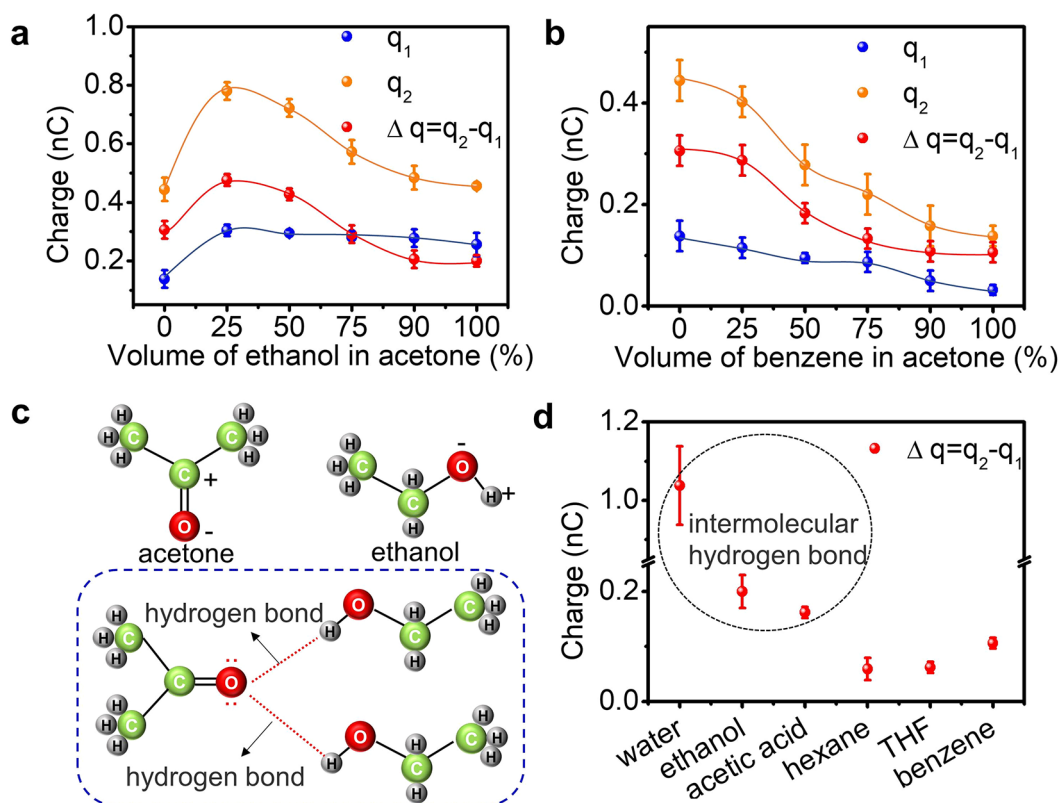
Figure 5. Sensing ability of droplet-TENG to the proportion of each solvent in the mixed organic solution. (a and b) The transferred charges on electrode 1 (q_1), electrode 2 (q_2), and charge between two electrodes (Δq) of acetone/ethanol and acetone/benzene mixed droplets sliding over the FEP surface, as a function of volume ratio of ethanol and benzene, respectively. (c) The electronic structures of acetone and ethanol and the intermolecular hydrogen bond generation when ethanol is added into acetone. (d) The transferred charge between two electrodes (Δq) for different droplets sliding over the FEP surface. Water, ethanol, and acetic acid with higher transferred charges enclosed in a circle can form intermolecular hydrogen bonds.

affinity to electrons[33] compared with PE and kapton; therefore, higher charge-transfer abilities were observed for FEP and PTFE. This also supports the electron transfer between the liquid−solid interface. Meanwhile, the acid, base, and salts with ion-rich droplets (take as an example, HCl (pH 3), NaOH (pH 13), and NaCl (0.5 M)) were also investigated as liquid droplets sliding across the FEP film. As seen from Figure 3f, the DI water droplet yielded the highest transferred charges, while the transferred charges between electrode 1 and 2 for the droplet with abundant ions are all smaller compared with that

of DI water. We also performed this experiment on the PTFE surface in Figure S5, and a similar trend was observed. The decrease of the contact electrification charge amount with the higher ion concentration can be attributed to the screen effect of free ions. For water, the ultralow ion concentration cannot fully support the ion transfer on the liquid−solid interface. However, the droplets with abundant ions (HCl, NaOH, and NaCl) lead to the excessive free ions in the droplets, which can interfere with the electron-transfer process because of the screen effect. Because the electron transfer dominates the

generation of charges, the excessive ions lead to the suppression of the charge amount. Different ions have different effects on the amounts of transferred charges between liquid and solid interfaces.[9,36] This reinforces that the electron transfer is dominant in the case of contact electrification between the liquid and a dielectric polymer interface.

To further confirm the electron transfer is dominant between the liquid−solid interface, organic droplets without any ions are also used in the experiments. The data in Figure 4a show evidence of the transferred charges generated between electrode 1 and electrode 2 even when the organic droplets are sliding across the FEP surface, for example, ethanol, acetone, hexane, tetrahydrofuran (THF), and benzene, which further highlights that electron transfer, instead of ion transfer, is dominant between the liquid−solid interface. Moreover, with the addition of ferrocene dissolved in the ethanol droplet, the transferred charges between electrode 1 and electrode 2 decrease as the concentration of ferrocene increases (Figure 4b). The highest concentration was chosen according to the solubility of the ferrocene in ethanol, and for comparison, a pure ethanol droplet was also used. It was reported that when there are more salt ions in an inorganic liquid, such as NaCl, fewer charges are transferred at the interface between the salt solution and a solid.[27] However, the relationship between the concentration of the organometallic compound with the transferred charge upon contact electrification is never revealed. Ferrocene is the most well-known organometallic[37] and is structurally characterized in Figure 4b as being like a "sandwich".[38] The physical−chemical properties of ferrocene and its derivatives lead themselves to application in a wide range of fields, including catalysis, materials science, and sensing, and it is an ideal internal standard in electrochemistry.[39] Thus, in our experiment we used ferrocene, the widely used organometallic compound, and depending on the decreasing of transferred charges between electrodes 1 and 2 when the ferrocene added into the ethanol droplet, we can probe trace amounts of ferrocene in an organic solvent, such as, 0.05 mg/mL in ethanol (Figure 4b), and this probe shows a high sensitivity to ferrocene.

In order to evaluate the performance of a droplet-TENG-based probe for the proportion of each solvent in the mixed organic solution, the transferred charges between electrode 1 and electrode 2 for acetone droplets with different volume ratio of ethanol and benzene were recorded separately (Figure 5a,b). As shown in Figure 5a, as the volume ratio of ethanol in the mixed solvent gradually increases (from 0% to 100%, note here 0% is pure acetone and 100% is pure ethanol), the amount of charge transferred between electrode 1 and electrode 2 shows a very surprising trend: the transferred charge reaches a maximum and then drops. When the volume ratio of ethanol in the mixed solution is less than 25%, the amount of transferred charges between electrode 1 and electrode 2 increases significantly compared with pure acetone and ethanol, but after that the transferred charge drops and is close to the transferred charge of pure ethanol when the ethanol volume ratio is up to 90% (Figure 5a). However, when benzene is added to acetone, there was no maximum peak observed. In contrast, as the volume ratio of benzene in the mixed solvent increases from 0% (pure acetone) to 100% (pure benzene), the amount of charge transferred gradually decreases until it is almost the same as that of benzene (Figure 5b). For these two different organic solvents added in the acetone droplet, ethanol and benzene, the transferred charges

generated by contact electrification are all changed compared with pure acetone. This shows that such a droplet-TENG with two electrodes is a high-sensitivity probe that can be used to analyze the percentage of each solvent in the organic mixed solvent.

However, the two curves in Figure 5a,b do not run similarly to each other; one has a peak but the other does not, as would be the case if the intermolecular force between molecules is a key factor guiding the charge transfer between the organic droplet and the dielectric polymer interface. Direct evidence of a relationship between intermolecular hydrogen bonding and the attainable amount of charge transfer between the organic droplet and dielectric polymer has never been reported. The different curves in Figure 5a,b probably would predict the relationship between intermolecular hydrogen bonding and charge transfer. A hydrogen bond is an intermolecular force that forms a special type of dipole−dipole attraction when a hydrogen atom bonded to a strongly electronegative atom exists in the vicinity of another electronegative atom with a lone pair of electrons.[40] Therefore, the electronic structure of acetone is a strongly electronegative atom O with two pairs of lone electrons (Figure 5c); thus, it is easy to form an intermolecular hydrogen bond with ethanol, with a hydrogen atom bonded to a strongly electronegative atom O. The existence of hydrogen bonds probably makes impurity states appear on the basis of the original molecular orbitals,[41] which is similar to the generation of surface states of a solid material. This probably accounts for the increasing of transferred charge in Figure 5a. In Figure 5a, the transferred charge between electrode 1 and electrode 2 increases significantly first, this is probably because the addition of a small amount of ethanol causes the formation of intermolecular hydrogen bonds between ethanol and acetone molecules. However, when the volume ratio of ethanol in the mixed solution is greater than 25%, the transferred charge drops, which could be attributed to the large number of ethanol molecules forming hydrogen bonds by themselves, resulting in a gradual decrease in the proportion of intermolecular hydrogen bonds between ethanol and acetone. On the other hand, because C−H in benzene is not a very polar bond, the hydrogen atom on benzene does not have enough positive protons and cannot be used as a hydrogen bond donor. This is probably the reason why adding benzene in the acetone droplet leads to the decreasing of transferred charge (Figure 5b). Moreover, molecules that can generate intermolecular hydrogen bonds by themselves have higher transferred charges, for example, water, ethanol, and acetic acid (Figure 5d) in comparison with hexane, THF, and benzene. Hence, it is possible that hydrogen bonding will enhance the charge transfer between the droplet and dielectric polymer.

CONCLUSION

We have developed a droplet-TENG with two spatially arranged electrodes for probing the charge transfer at the dielectric liquid−solid interface. The approach relies on the analysis of the induced charge on copper electrodes generated by the droplet sliding over a certain distance on the dielectric polymer surface. Both ionic and organic droplets were considered in our experiments. Taken together these findings constitute the most compelling evidence to date for the charge transfer between liquid and solid interface in dielectric polymers being electrons. The relationship between the concentration of organometallic compound (ferrocene) with

the transferred charge upon contact electrification was studied, which established an efficient chemical sensor based on the droplet-TENG to probe the traces of organic impurities in solvents. Moreover, in the course of this work we have discovered that the molecules which can generate intermolecular hydrogen bonds have higher transferred charges, showing the hydrogen bond is probably a significant factor impacting charge transfer between the liquid—solid interface, and this type of droplet-TENG could be a sensor for detecting intramolecular forces of organic compounds. This work extends our understanding of static electricity for liquid—solid interfaces and may find applications in chemical sensing[42] and single-electrode electrochemistry.[43]

EXPERIMENTAL SECTION

Materials. Redistilled solvents and Milli-Q water (>18 MΩ cm) were used for substrate cleaning and to prepare solutions. Films of fluorinated ethylene propylene (FEP, 30 μm, DAIKIN), polytetra-fluoroethylene (PTFE, 80 μm, ASF-110 FR, Chukoh Company), kapton (100 μm, Botron), and polyethylene (PE, 50 μm, Xingweifeng Technology Co., Ltd.) were used to contact with the liquid droplet. Hydrochloric acid (37%), sodium hydroxide (97%), sodium chloride (99%), and ferrocene (98%) were purchased from Sigma. Ethanol (99.7%), acetone (99.5%), THF (99%), and acetic acid (99.5%) were obtained from Yong Da Chemical. Hexane (97%) and benzene (99.7%) were purchased from Aladdin.

Fabrication of Droplet-TENG. Plastic films were extensively washed with ethanol prior to each experiment to remove static charges. Two copper electrodes (copper films, 2×6 cm^2, thickness of 30 μm) were attached on a smooth and clean poly(methyl methacrylate) (PMMA) plate ($6 \times 16 \times 0.5$ cm^3) separately; PMMA plate were used as the backboards. After the copper electrodes were attached, the plastic films were carefully attached on the PMMA plate. Note that the attached plastic film must cover all areas of the copper film attached to the PMMA plate to avoid electrical interference and chemical corrosion.

Electrical Measurement. Two copper electrodes attached on the PMMA plate were connected to two Keithley 6514 electrometers, separately. The Keithley 6514 electrometers with a Labview program on a computer were used to measure the induced currents on the two copper electrodes produced by the interaction between the droplet and the plastic and operating on the nA scale. When a droplet contacts or separates from the copper electrode, a current peak appears on the Labview interface. These data correspond to changes in the surface charge of the polymer. Notably, unless otherwise specified, the droplet height was 0.8 cm and the air humidity was 30%. The liquid droplet was dripped by a syringe pump (PHD ULTRA Series, Harvard Apparatus) and was grounded in the experiment.

ASSOCIATED CONTENT

ⓢ Supporting Information

The Supporting Information is available free of charge at https://pubs.acs.org/doi/10.1021/acsnano.1c04903.

Additional photos of water droplets at different dropping angle, contact angle data, and additional electricity performance for hundreds of water droplets (PDF)

AUTHOR INFORMATION

Corresponding Author

Zhong Lin Wang − *Beijing Institute of Nanoenergy and Nanosystems, Chinese Academy of Sciences, Beijing 100083, P.R. China; School of Nanoscience and Technology, University of Chinese Academy of Sciences, Beijing 100049, P.R. China; School of Materials Science and Engineering, Georgia Institute of Technology, Atlanta, Georgia*

30332−0245, United States; ⓞ orcid.org/0000-0002-5530-0380; Email: zlwang@gatech.edu

Authors

Jinyang Zhang − *Beijing Institute of Nanoenergy and Nanosystems, Chinese Academy of Sciences, Beijing 100083, P.R. China; School of Nanoscience and Technology, University of Chinese Academy of Sciences, Beijing 100049, P.R. China*

Shiquan Lin − *Beijing Institute of Nanoenergy and Nanosystems, Chinese Academy of Sciences, Beijing 100083, P.R. China; School of Nanoscience and Technology, University of Chinese Academy of Sciences, Beijing 100049, P.R. China*

Mingli Zheng − *Beijing Institute of Nanoenergy and Nanosystems, Chinese Academy of Sciences, Beijing 100083, P.R. China; School of Nanoscience and Technology, University of Chinese Academy of Sciences, Beijing 100049, P.R. China*

Complete contact information is available at:
https://pubs.acs.org/10.1021/acsnano.1c04903

Author Contributions

§J.Z. and S.L. contributed equally to this work.

Notes

The authors declare no competing financial interest.

REFERENCES

(1) Zhang, J.; Su, C.; Rogers, F.; Darwish, N.; Coote, M.; Ciampi, S. Irreproducibility in the Triboelectric Charging of Insulators: Evidence of a Non-Monotonic Charge *versus* Contact Time Relationship. *Phys. Chem. Chem. Phys.* **2020**, *22*, 11671−11677.

(2) Zhang, J.; Ciampi, S. Shape and Charge: Faraday's Ice Pail Experiment Revisited. *ACS Cent. Sci.* **2020**, *6*, 611−612.

(3) Baytekin, H.; Patashinski, A.; Branicki, M.; Baytekin, B.; Soh, S.; Grzybowski, B. A. The Mosaic of Surface Charge in Contact Electrification. *Science* **2011**, *333*, 308−312.

(4) Zhang, J.; Ferrie, S.; Zhang, S.; Vogel, Y. B.; Peiris, C.; Darwish, N.; Ciampi, S. Single-Electrode Electrochemistry: Chemically Engineering Surface Adhesion and Hardness to Maximize Redox Work Extracted from Tribocharged Silicon. *ACS Appl. Nano Mater.* **2019**, *2*, 7230−7236.

(5) Apodaca, M. M.; Wesson, P. J.; Bishop, K. J.; Ratner, M. A.; Grzybowski, B. A. Contact Electrification between Identical Materials. *Angew. Chem., Int. Ed.* **2010**, *49*, 946−949.

(6) Castle, G. Contact Charging between Insulators. *J. Electrost.* **1997**, *40*, 13−20.

(7) Iversen, P.; Lacks, D. J. A Life of Its Own: The Tenuous Connection between Thales of Miletus and the Study of Electrostatic Charging. *J. Electrost.* **2012**, *70*, 309−311.

(8) Childress, C. O.; Kabell, L. J. Electrostatic Printing System. US 3081698163, 1963.

(9) Nie, J.; Ren, Z.; Xu, L.; Lin, S.; Zhan, F.; Chen, X.; Wang, Z. L. Probing Contact-Electrification-Induced Electron and Ion Transfers at a Liquid−Solid Interface. *Adv. Mater.* **2020**, *32*, 1905696.

(10) Liu, Z.; Ma, Y.; Ouyang, H.; Shi, B.; Li, N.; Jiang, D.; Xie, F.; Qu, D.; Zou, Y.; Huang, Y.; et al. Endocardial Pressure Sensors: Transcatheter Self-Powered Ultrasensitive Endocardial Pressure Sensor. *Adv. Funct. Mater.* **2019**, *29*, 1970017.

(11) Shahzad, A.; Wijewardhana, K. R.; Song, J.-K. Contact Electrification Efficiency Dependence on Surface Energy at the Water-Solid Interface. *Appl. Phys. Lett.* **2018**, *113*, No. 023901.

(12) Yin, J.; Zhang, Z.; Li, X.; Zhou, J.; Guo, W. Harvesting Energy from Water Flow over Graphene? *Nano Lett.* **2012**, *12*, 1736−1741.

(13) Diaz, A. F.; Guay, J. Contact Charging of Organic Materials: Ion *vs.* Electron Transfer. *IBM J. Res. Dev.* **1993**, *37*, 249−260.

(14) Davies, D. Charge Generation on Dielectric Surfaces. *J. Phys. D: Appl. Phys.* **1969**, *2*, 1533−1537.

(15) Liu, Y.; Zheng, Y.; Li, T.; Wang, D.; Zhou, F. Water-Solid Triboelectrification with Self-Repairable Surfaces for Water-Flow Energy Harvesting. *Nano Energy* **2019**, *61*, 454−461.

(16) Li, X.; Zhang, L.; Feng, Y.; Zhang, X.; Wang, D.; Zhou, F. Solid−Liquid Triboelectrification Control and Antistatic Materials Design Based on Interface Wettability Control. *Adv. Funct. Mater.* **2019**, *29*, 1903587.

(17) Zhang, J.; Rogers, F.; Darwish, N.; Gonçales, V. R.; Vogel, Y. B.; Wang, F.; Gooding, J. J.; Peiris, M. C.; Jia, G.; Veder, J.-P.; Coote, M. L.; Ciampi, S. Electrochemistry on Tribocharged Polymers Is Governed by the Stability of Surface Charges Rather than Charging Magnitude. *J. Am. Chem. Soc.* **2019**, *141*, 5863−5870.

(18) Byun, K.-E.; Cho, Y.; Seol, M.; Kim, S.; Kim, S.-W.; Shin, H.-J.; Park, S.; Hwang, S. Control of Triboelectrification by Engineering Surface Dipole and Surface Electronic State. *ACS Appl. Mater. Interfaces* **2016**, *8*, 18519−18525.

(19) Liu, C.-y.; Bard, A. J. Electrons on Dielectrics and Contact Electrification. *Chem. Phys. Lett.* **2009**, *480*, 145−156.

(20) Liu, C.; Bard, A. J. Electrostatic Electrochemistry at Insulators. *Nat. Mater.* **2008**, *7*, 505−509.

(21) Tang, W.; Chen, B. D.; Wang, Z. L. Recent Progress in Power Generation from Water/Liquid Droplet Interaction with Solid Surfaces. *Adv. Funct. Mater.* **2019**, *29*, 1901069.

(22) Chatterjee, S.; Burman, S. R.; Khan, I.; Saha, S.; Choi, D.; Lee, S.; Lin, Z.-H. Recent Advancements in Solid−Liquid Triboelectric Nanogenerators for Energy Harvesting and Self-Powered Applications. *Nanoscale* **2020**, *12*, 17663−17697.

(23) Moon, J. K.; Jeong, J.; Lee, D.; Pak, H. K. Electrical Power Generation by Mechanically Modulating Electrical Double Layers. *Nat. Commun.* **2013**, *4*, 1487.

(24) Lee, J. H.; Kim, S.; Kim, T. Y.; Khan, U.; Kim, S.-W. Water Droplet-Driven Triboelectric Nanogenerator with Superhydrophobic Surfaces. *Nano Energy* **2019**, *58*, 579−584.

(25) Yang, L.; Wang, Y.; Guo, Y.; Zhang, W.; Zhao, Z. Robust Working Mechanism of Water Droplet-Driven Triboelectric Nanogenerator: Triboelectric Output *versus* Dynamic Motion of Water Droplet. *Adv. Mater. Interfaces* **2019**, *6*, 1901547.

(26) Yang, L.; Wang, Y.; Zhao, Z.; Guo, Y.; Chen, S.; Zhang, W.; Guo, X. Particle-Laden Droplet-Driven Triboelectric Nanogenerator for Real-Time Sediment Monitoring Using a Deep Learning Method. *ACS Appl. Mater. Interfaces* **2020**, *12*, 38192−38201.

(27) Zhan, F.; Wang, A. C.; Xu, L.; Lin, S.; Shao, J.; Chen, X.; Wang, Z. L. Electron Transfer as a Liquid Droplet Contacting a Polymer Surface. *ACS Nano* **2020**, *14*, 17565−17573.

(28) Zhong, W.; Xu, L.; Zhan, F.; Wang, H.; Wang, F.; Wang, Z. L. Dripping Channel Based Liquid Triboelectric Nanogenerators for Energy Harvesting and Sensing. *ACS Nano* **2020**, *14*, 10510−10517.

(29) Xu, L.; Pang, Y.; Zhang, C.; Jiang, T.; Chen, X.; Luo, J.; Tang, W.; Cao, X.; Wang, Z. L. Integrated Triboelectric Nanogenerator Array Based on Air-Driven Membrane Structures for Water Wave Energy Harvesting. *Nano Energy* **2017**, *31*, 351−358.

(30) Zhong, W.; Xu, L.; Yang, X.; Tang, W.; Shao, J.; Chen, B.; Wang, Z. L. Open-Book-Like Triboelectric Nanogenerators Based on Low-Frequency Roll−Swing Oscillators for Wave Energy Harvesting. *Nanoscale* **2019**, *11*, 7199−7208.

(31) Xiao, T. X.; Liang, X.; Jiang, T.; Xu, L.; Shao, J. J.; Nie, J. H.; Bai, Y.; Zhong, W.; Wang, Z. L. Spherical Triboelectric Nanogenerators Based on Spring-Assisted Multilayered Structure for Efficient Water Wave Energy Harvesting. *Adv. Funct. Mater.* **2018**, *28*, 1802634.

(32) Niu, S.; Wang, S.; Liu, Y.; Zhou, Y. S.; Lin, L.; Hu, Y.; Pradel, K. C.; Wang, Z. L. A Theoretical Study of Grating Structured Triboelectric Nanogenerators. *Energy Environ. Sci.* **2014**, *7*, 2339−2349.

(33) Chen, A.; Zhang, C.; Zhu, G.; Wang, Z. L. Polymer Materials for High-Performance Triboelectric Nanogenerators. *Adv. Sci.* **2020**, *7*, 2000186.

(34) Gauduel, Y.; Pommeret, S.; Migus, A.; Antonetti, A. Some Evidence of Ultrafast H_2O^+-Water Molecule Reaction in Femtosecond Photoionization of Pure Liquid Water: Influence on Geminate Pair Recombination Dynamics. *Chem. Phys.* **1990**, *149*, 1−10.

(35) Loh, Z.-H.; Doumy, G.; Arnold, C.; Kjellsson, L.; Southworth, S.; Al Haddad, A.; Kumagai, Y.; Tu, M.-F.; Ho, P.; March, A. Observation of the Fastest Chemical Processes in the Radiolysis of Water. *Science* **2020**, *367*, 179−182.

(36) Lin, S.; Xu, L.; Wang, A. C.; Wang, Z. L. Quantifying Electron-Transfer in Liquid-Solid Contact Electrification and the Formation of Electric Double-Layer. *Nat. Commun.* **2020**, *11*, 399.

(37) Laszlo, P.; Hoffmann, R. Ferrocene: Ironclad History or Rashomon Tale? *Angew. Chem., Int. Ed.* **2000**, *39*, 123−124.

(38) Patra, M.; Gasser, G. The Medicinal Chemistry of Ferrocene and Its Derivatives. *Nat. Rev. Chem.* **2017**, *1*, 0066.

(39) Stepnicka, P. *Ferrocenes: Ligands, Materials and Biomolecules*; John Wiley & Sons Ltd.: Chichester, U.K., 2008.

(40) Kollman, P. A.; Allen, L. C. Theory of the Hydrogen Bond. *Chem. Rev.* **1972**, *72*, 283−303.

(41) Lin, S.; Zheng, M.; Luo, J.; Wang, Z. L. Effects of Surface Functional Groups on Electron Transfer at Liquid−Solid Interfacial Contact Electrification. *ACS Nano* **2020**, *14*, 10733−10741.

(42) Ying, Z.; Long, Y.; Yang, F.; Dong, Y.; Li, J.; Zhang, Z.; Wang, X. Self-Powered Liquid Chemical Sensors Based on Solid−Liquid Contact Electrification. *Analyst* **2021**, *146*, 1656−1662.

(43) Zhao, X. J.; Kuang, S. Y.; Wang, Z. L.; Zhu, G. Electricity− Free Electroluminescence Excited by Droplet Impact Driven Triboelectric Field on Solid− Liquid Interface. *Nano Energy* **2020**, *75*, 104823.